



CHALMERS

Chalmers Publication Library

A 2D model of ultrasonic testing for cracks near a non-planar surface

This document has been downloaded from Chalmers Publication Library (CPL). It is the author's version of a work that was accepted for publication in:

Wave motion (ISSN: 0165-2125)

Citation for the published paper:

Westlund, J. ; Boström, A. (2010) "A 2D model of ultrasonic testing for cracks near a non-planar surface". Wave motion, vol. 47(6), pp. 383-394.

<http://dx.doi.org/10.1016/j.wavemoti.2009.12.004>

Downloaded from: <http://publications.lib.chalmers.se/publication/122949>

Notice: Changes introduced as a result of publishing processes such as copy-editing and formatting may not be reflected in this document. For a definitive version of this work, please refer to the published source. Please note that access to the published version might require a subscription.

Chalmers Publication Library (CPL) offers the possibility of retrieving research publications produced at Chalmers University of Technology. It covers all types of publications: articles, dissertations, licentiate theses, masters theses, conference papers, reports etc. Since 2006 it is the official tool for Chalmers official publication statistics. To ensure that Chalmers research results are disseminated as widely as possible, an Open Access Policy has been adopted. The CPL service is administrated and maintained by Chalmers Library.

(article starts on next page)

A 2D MODEL OF ULTRASONIC TESTING FOR CRACKS NEAR A NON-PLANAR SURFACE

J. WESTLUND, A. BOSTRÖM

ABSTRACT. 2D P-SV elastic wave scattering by a crack near a non-planar surface is investigated. The solution method employed is based on a reformulation of the wave scattering problem as two coupled boundary integral equations (BIE): a traction BIE for the crack opening displacement (COD) and a displacement BIE for the back surface displacement. The two coupled integral equations are solved using a combination of the boundary element method (BEM) for the back surface and a series expansion of the COD in Chebyshev functions. To model an ultrasonic contact probe in transmission, the traction on the surface beneath the probe is prescribed. The action of the receiving ultrasonic probe is modelled using a reciprocity relation. A few numerical examples illustrating the influence of the back surface are given.

1. INTRODUCTION

The propagation of elastic waves and scattering by defects have important applications in nondestructive testing (NDT) and evaluation (NDE), for instance in the nuclear power and aerospace industries. Many efforts have therefore been directed towards modelling of such scattering processes. A good and validated model has several important uses. It is easy to perform parametric studies with a model, and in this way costly experiments can be kept to a minimum. A model is also a valuable tool when testing procedures are developed and optimized. A model gives an increased understanding of the ultrasonic wave propagation and scattering and is also useful in qualification work.

The most important and critical defect is a crack and a lot of work has been done on the scattering by cracks. However, not so much effort has been put into the modelling of the whole NDT situation, including also models of ultrasonic probes in transmission and reception and the calibration by some standard reflector, such as a side-drilled hole. Chapman [1] and Calmon et al. [2] use combinations of the Geometrical Theory of Diffraction and the Kirchhoff approximation to consider quite general geometries, but it is hard to tell how well these approximations work in a particular case. Bøvik and Boström [3] employ a hypersingular integral equation method to investigate the scattering by a strip-like crack with a close planar back surface, the results then being in essence exact.

The purpose of the present work is to investigate the scattering by a crack close to a non-planar back surface, i.e. the surface opposite to the scanning surface. This is a situation that occurs in applications such as the testing of thick-walled pipes, with a diameter change or

a connection, in the nuclear power industry. The combination of a crack and a non-planar back surface complicates the ultrasonic testing because the signal from the crack may be masked by the signal from the non-planar surface. The 2D in-plane case is considered in this paper and this is an extension of the earlier work by Westlund [4], where the corresponding antiplane case is studied. The employed solution method is a combination of a displacement boundary integral equation (BIE) for the back surface displacement and a hypersingular traction BIE for the crack opening displacement. This gives a very effective treatment of the crack while allowing a general geometry of the back surface, and since the method is essentially exact the model provides accurate results for both high and low frequencies.

The plan of the present paper is as follows. In section 2 the scattering problem is formulated and in section 3 the different Green's tensors are discussed. In section 4 the two integral equations are derived starting from an integral representation. Section 5 describes the modelling of ultrasonic probes in transmission and reception. In section 6 the discretization of the integral equations is stated and in section 7 the numerical treatment is discussed and a few numerical examples given. Section 8 offers some concluding remarks.

2. PROBLEM FORMULATION

Consider a 2D scattering geometry as depicted in Fig. 1, where an interior strip-like crack of width $2a$ is located in a thick-walled component with a non-planar back surface. In the exterior of the crack the component is isotropic and homogeneous with Lamé constants λ and μ and density ρ . The inclination of the crack with respect to the horizontal is given by the angle β .

Figure 1 also introduces two coordinate systems: the crack coordinate system (x_1, x_2) and the back surface coordinate system (x_1^b, x_2^b) . The superscript 'b' on quantities indicate that they are represented in the back surface coordinate system. The standard transformation rules for the transformation between the two coordinate systems apply.

On the scanning surface of the component two ultrasonic contact probes are located: a transmitting ultrasonic probe (t) and a receiving ultrasonic probe (r). The half-widths of the probes are denoted w_t and w_r , respectively, and the positions of the probes in relation to the crack center are given by (t_1^b, t_2^b) and (r_1^b, r_2^b) in the coordinate system of the back surface. As a special case one probe can act as both transmitter and receiver in a pulse-echo testing situation.

The multiple scattering between the crack and the back surface is accounted for in the model, so the distance between them may be arbitrary as long as the crack is interior and not surface-breaking. However, the distance between the scanning surface of the component and the crack and back surface is assumed to be large enough (i.e. at least a couple of wavelengths) so that multiple scattering between these surfaces can be neglected.

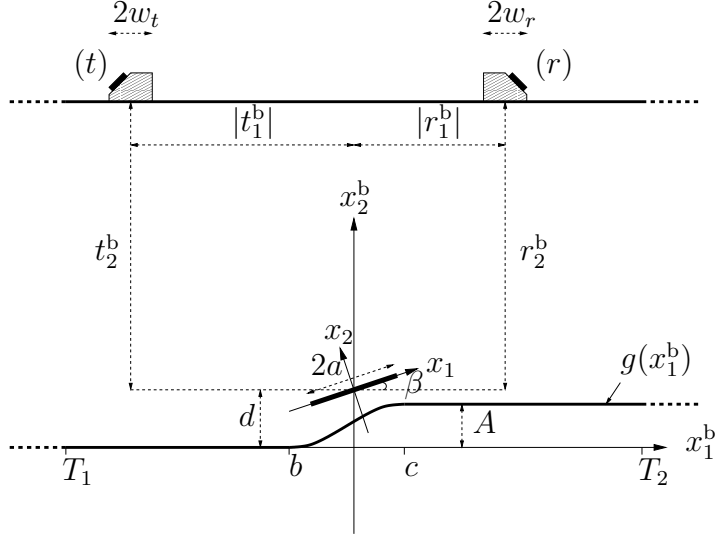


FIGURE 1. The geometry with an interior strip-like crack in a thick-walled component with a non-planar back surface.

To enable the subsequent boundary element discretization of the back surface, it is truncated at the left and right truncation limits T_1 and T_2 . The actual shape of the non-planar back surface $g(x_1^b)$ may be quite arbitrary as long as it has no cusps, as scattering by such cusps is not accounted for. The back surface is assumed to be planar to the left of some lower limit b and to the right of some upper limit c , and A is the vertical distance between the lower and upper parts of the back surface.

In 2D elastodynamics the wave motion decouples into two types: in-plane P and SV waves and antiplane SH waves. In this paper the coupled P-SV wave scattering problem is treated. Time-harmonic conditions are considered, and the time-factor $e^{-i\omega t}$ is suppressed throughout (where ω is the angular frequency and t the time). Under these conditions the equations of motion are:

$$\nabla \cdot \boldsymbol{\sigma} + \rho\omega^2 \mathbf{u} = \mathbf{0}, \quad (2.1)$$

where $\boldsymbol{\sigma}$ is the Cauchy stress tensor and \mathbf{u} the displacement. The Cauchy stress tensor is given in terms of the stiffness tensor \mathbf{C} and the displacement \mathbf{u} by Hooke's law:

$$\boldsymbol{\sigma} = \mathbf{C} : \nabla \mathbf{u}. \quad (2.2)$$

For the isotropic and homogeneous material considered the elastic stiffness tensor \mathbf{C} can be expressed as:

$$\mathbf{C} = \lambda \mathbf{I}_2 \otimes \mathbf{I}_2 + 2\mu \mathbf{S}_4, \quad (2.3)$$

where \mathbf{I}_2 is the second-order identity tensor and \mathbf{S}_4 the symmetric fourth-order identity tensor. By using the explicit form of the stiffness tensor (2.3) in Hooke's law (2.2), the equations of motion (2.1) can be rewritten on the familiar form:

$$k_p^{-2} \nabla (\nabla \cdot \mathbf{u}) - k_s^{-2} \nabla \times (\nabla \times \mathbf{u}) + \mathbf{u} = \mathbf{0}, \quad (2.4)$$

where $k_p = \omega/c_p$ is the pressure wave number, $c_p = \sqrt{(\lambda + 2\mu)/\rho}$ the pressure wave speed, $k_s = \omega/c_s$ the shear wave number and $c_s = \sqrt{\mu/\rho}$ the shear wave speed.

The crack is open and thus traction-free, and the back surface is also free of tractions. In addition, the scanning surface of the component is free of tractions except for the action of the ultrasonic probes which is discussed in section 5. Letting C_{BS} denote the back surface, \mathbf{e}_2 the unit normal vector in the 2-direction of the coordinate system of the crack and \mathbf{n} the downward unit normal vector on C_{BS} , the boundary conditions on the crack and back surface are thus:

$$\begin{cases} \lim_{x_2 \rightarrow 0^+} \boldsymbol{\sigma}(\mathbf{x}) \cdot \mathbf{e}_2 = \lim_{x_2 \rightarrow 0^-} \boldsymbol{\sigma}(\mathbf{x}) \cdot \mathbf{e}_2 = \mathbf{0}, & |x_1| < a \\ \boldsymbol{\sigma}(\mathbf{x}) \cdot \mathbf{n} = \mathbf{0}, & (x_1, x_2) \in C_{BS}. \end{cases} \quad (2.5)$$

It should be noted that since \mathbf{u} is discontinuous across the crack the boundary condition on the crack must be taken as a limit as the point approaches the crack, from either side.

3. THE GREEN'S TENSORS

The solution method employed in this paper reformulates the wave scattering problem as two coupled boundary integral equations, which are subsequently solved simultaneously. The reformulation is based on the use of the outward propagating Green's tensor for the infinite plane. In the following, the outward propagating Green's displacement tensor is denoted $\mathbf{U}^k(\mathbf{x}, \mathbf{y}; \omega)$. The corresponding stress tensor, denoted $\boldsymbol{\Sigma}^k(\mathbf{x}, \mathbf{y}; \omega)$, is calculated by applying Hooke's law (2.2) to the displacement tensor $\mathbf{U}^k(\mathbf{x}, \mathbf{y}; \omega)$, i.e. $\boldsymbol{\Sigma}^k(\mathbf{x}, \mathbf{y}; \omega) = \mathbf{C} : \nabla \mathbf{U}^k(\mathbf{x}, \mathbf{y}; \omega)$. Here and throughout, the ∇ -operator always acts on the \mathbf{x} -coordinates unless otherwise specified.

The Green's tensor, also called the Helmholtz fundamental solution in plane strain, is the outward propagating solution to the equation:

$$\nabla \cdot \boldsymbol{\Sigma}^k(\mathbf{x}, \mathbf{y}; \omega) + \rho\omega^2 \mathbf{U}^k(\mathbf{x}, \mathbf{y}; \omega) = -\delta(\mathbf{x} - \mathbf{y})\mathbf{e}_k \quad (3.1)$$

where $\delta(\mathbf{x} - \mathbf{y})$ is the 2D Dirac delta distribution and \mathbf{e}_k the unit vector in the k -direction of the coordinate system of the crack. The Green's tensor is easily computed using the formula (for a derivation see e.g. Ström [5]):

$$\begin{aligned} U_j^k(\mathbf{x}, \mathbf{y}; \omega) = & \frac{i}{4\mu k_s^2} \left[k_s^2 \delta_{jk} H_0^{(1)}(k_s |\mathbf{x} - \mathbf{y}|) \right. \\ & \left. + \frac{\partial}{\partial x_j} \frac{\partial}{\partial x_k} \left(H_0^{(1)}(k_s |\mathbf{x} - \mathbf{y}|) - H_0^{(1)}(k_p |\mathbf{x} - \mathbf{y}|) \right) \right], \end{aligned} \quad (3.2)$$

where δ_{jk} is the Kronecker delta and $H_0^{(1)}$ the Hankel function of the first kind and zeroth order.

The solution method also employs the Fourier integral representation of the Green's tensor. This representation can be derived by expanding the Green's tensor in plane P and

SV waves and using the jump conditions introduced by the presence of the Dirac delta distribution on the right-hand side of Eq. (3.1). Alternatively, Eq. (3.2) may be used in conjunction with the following Fourier integral representation of the Hankel function:

$$H_0^{(1)}(k_j|\mathbf{x} - \mathbf{y}|) = \frac{1}{\pi} \int_{-\infty}^{\infty} \frac{1}{h_j} e^{i(q(x_1 - y_1) + h_j|x_2 - y_2|)} dq, \quad (3.3)$$

where $j = p, s$ and $h_j = h_j(q) = \sqrt{k_j^2 - q^2}$. Here and throughout, the branch of the complex square root is chosen such that $\text{Im} \sqrt{z} \geq 0 \forall z \in \mathbb{C}$.

The regularization process employed in section 4 makes use of the static Green's displacement tensor for the infinite plane, denoted $\mathbf{U}^k(\mathbf{x}, \mathbf{y})$ with corresponding static Green's stress tensor $\boldsymbol{\Sigma}^k(\mathbf{x}, \mathbf{y}) = \mathbf{C} : \nabla \mathbf{U}^k(\mathbf{x}, \mathbf{y})$. The static Green's tensor, also called the Kelvin fundamental solution in plane strain, is the corresponding solution of (3.1) for $\omega = 0$. It is given explicitly by e.g. Bonnet [6].

4. THE INTEGRAL EQUATIONS

In this section the Green's tensors are used to reformulate the wave scattering problem as two coupled boundary integral equations (BIEs): one BIE for the back surface and one for the crack. The unknowns are the crack opening displacement (COD), i.e. the displacement jump over the crack, and the back surface displacement.

4.1. The integral equation for the back surface. The BIE for the back surface is derived from an application of the 2D divergence theorem. Since the multiple scattering between the scanning surface of the component and the crack and back surface is neglected, the scattering by a crack in a half-plane with a non-planar back surface is the problem to be solved. To this end consider a closed contour $C_r + C_{\varepsilon, r} + C_\varepsilon + C_{\delta_1, \delta_2} + C_i$ as depicted in Fig. 4.1, where \mathbf{y} is an arbitrary point on the back surface C_{BS} . Here C_r is a semicircle of radius r with center at \mathbf{y} , and $C_{\varepsilon, r}$ is the part of the back surface within the distance r from \mathbf{y} but with a neighborhood around \mathbf{y} excluded. C_ε is an exclusion neighborhood of arbitrary shape and a radius $\leq \varepsilon$. The exclusion neighborhood around \mathbf{y} is necessary since the integrand is singular at \mathbf{y} . C_{δ_1, δ_2} is a closed contour containing the crack with circular arcs of radius δ_2 centered at the crack tips, and straight lines parallel with the crack at a distance δ_1 (with $\delta_1 < \delta_2$) from it. C_i is a closed contour containing the source of the incoming field, i.e. the transmitting probe.

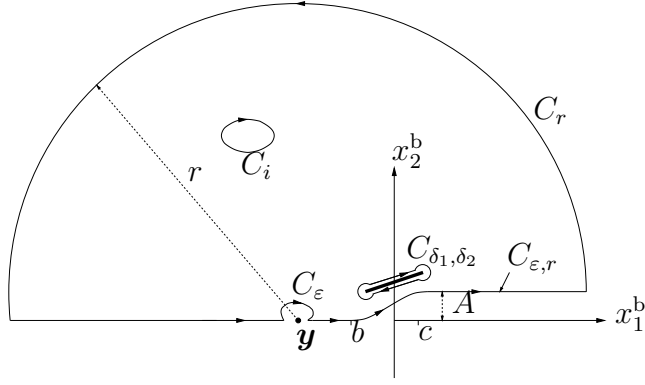


FIGURE 2. The integration contour used in the derivation of the integral equation for the back surface.

Integration of $\mathbf{U}^k \cdot (2.1) - \mathbf{u} \cdot (3.1)$ over the closed contour $C_r + C_{\epsilon, r} + C_\epsilon + C_{\delta_1, \delta_2} + C_i$, letting first $\delta_1 \rightarrow 0^+$ and then $\delta_2 \rightarrow 0^+$, yields after invoking the boundary conditions:

$$\begin{aligned}
& \int_{C_r} [U_i^k(\mathbf{x}, \mathbf{y}; \omega) \sigma_{ij}(\mathbf{x}) - u_i(\mathbf{x}) \Sigma_{ij}^k(\mathbf{x}, \mathbf{y}; \omega)] n_j(\mathbf{x}) ds_x \\
& - \int_{C_{\epsilon, r} + C_\epsilon} u_i(\mathbf{x}) \Sigma_{ij}^k(\mathbf{x}, \mathbf{y}; \omega) n_j(\mathbf{x}) ds_x \\
& + \int_{-a}^a \Delta u_i(x_1) \Sigma_{i2}^k(x_1, 0, \mathbf{y}; \omega) dx_1 + u_k^{\text{in}}(\mathbf{y}) = 0.
\end{aligned} \tag{4.1}$$

Here u_k^{in} is the k :th component of the incoming field from the transmitting probe in the absence of the crack and back surface, Δu_i is the COD: $\Delta u_i(x_1) \equiv u_i(x_1, 0^+) - u_i(x_1, 0^-)$ and $k = 1, 2$.

The limit $\epsilon \rightarrow 0^+$ is to be considered next. In this limit the integrand in the integral over $C_{\epsilon, r} + C_\epsilon$ becomes strongly singular [7]. The integral over C_ϵ then gives rise to a so-called free-term, and the strongly singular integral over the back surface must be interpreted in the sense of a Cauchy principal value integral. In order to avoid the difficulties associated with the numerical computation of strongly singular integrals, an indirect regularization approach (in the nomenclature of Bonnet [6]) is employed in this paper. To this end the terms $u_i(\mathbf{x}) \Sigma_{ij}^k(\mathbf{x}, \mathbf{y})$ and $u_i(\mathbf{y}) \Sigma_{ij}^k(\mathbf{x}, \mathbf{y})$ in the integral over $C_{\epsilon, r} + C_\epsilon$ are subtracted and

added back to yield:

$$\begin{aligned}
& \int_{C_r} [U_i^k(\mathbf{x}, \mathbf{y}; \omega) \sigma_{ij}(\mathbf{x}) - u_i(\mathbf{x}) \Sigma_{ij}^k(\mathbf{x}, \mathbf{y}; \omega)] n_j(\mathbf{x}) ds_x \\
& - \int_{C_{\varepsilon, r} + C_{\varepsilon}} u_i(\mathbf{x}) [\Sigma_{ij}^k(\mathbf{x}, \mathbf{y}; \omega) - \Sigma_{ij}^k(\mathbf{x}, \mathbf{y})] n_j(\mathbf{x}) ds_x \\
& - \int_{C_{\varepsilon, r} + C_{\varepsilon}} [u_i(\mathbf{x}) - u_i(\mathbf{y})] \Sigma_{ij}^k(\mathbf{x}, \mathbf{y}) n_j(\mathbf{x}) ds_x \\
& - u_i(\mathbf{y}) \int_{C_{\varepsilon, r} + C_{\varepsilon}} \Sigma_{ij}^k(\mathbf{x}, \mathbf{y}) n_j(\mathbf{x}) ds_x \\
& + \int_{-a}^a \Delta u_i(x_1) \Sigma_{i2}^k(x_1, 0, \mathbf{y}; \omega) dx_1 + u_k^{\text{in}}(\mathbf{y}) = 0.
\end{aligned} \tag{4.2}$$

Since the singular behaviour of $\Sigma^k(\mathbf{x}, \mathbf{y}; \omega)$ and $\Sigma^k(\mathbf{x}, \mathbf{y})$ is the same, the first integral over $C_{\varepsilon, r} + C_{\varepsilon}$ is regular. Granted that the displacement \mathbf{u} satisfies the usual assumption of Hölder continuity [6, 8], i.e. $\mathbf{u} \in \mathcal{C}^{0, \alpha}$ with $0 < \alpha \leq 1$, the second integral over $C_{\varepsilon, r} + C_{\varepsilon}$ is weakly singular. In the limit $\varepsilon \rightarrow 0^+$, these two integrals over C_{ε} hence vanish and the integrals over $C_{\varepsilon, r}$ become ordinary integrals over $C_{BS, r}$, i.e. over the back surface extending to a distance r from \mathbf{y} and without an exclusion neighborhood around \mathbf{y} . The third and strongly singular integral over $C_{\varepsilon, r} + C_{\varepsilon}$ remains. However, by using the 2D divergence theorem this integral can be transformed to an integral over C_r which can be evaluated analytically.

The limit $r \rightarrow \infty$ must also be considered. Since the Green's tensor of the infinite plane is used, it satisfies an appropriate radiation condition. For a physically reasonable displacement \mathbf{u} and associated stress $\boldsymbol{\sigma}$, the integral over C_r must then vanish when $r \rightarrow \infty$. Further, after transforming the strongly singular integral over $C_{\varepsilon, r} + C_{\varepsilon}$ to an integral over C_r and evaluating it analytically, one obtains:

$$\lim_{r \rightarrow \infty} \int_{C_{\varepsilon, r} + C_{\varepsilon}} \Sigma_{ij}^k(\mathbf{x}, \mathbf{y}) n_j(\mathbf{x}) ds_x = \frac{1}{2} \delta_{ik}. \tag{4.3}$$

Letting $C_{BS, \infty}$ denote the back surface extending to infinity (i.e. not truncated), in the limit $r \rightarrow \infty, \varepsilon \rightarrow 0^+$ Eq. (4.2) then yields:

$$\begin{aligned}
& - \int_{C_{BS, \infty}} u_i(\mathbf{x}) [\Sigma_{ij}^k(\mathbf{x}, \mathbf{y}; \omega) - \Sigma_{ij}^k(\mathbf{x}, \mathbf{y})] n_j(\mathbf{x}) ds_x \\
& - \int_{C_{BS, \infty}} [u_i(\mathbf{x}) - u_i(\mathbf{y})] \Sigma_{ij}^k(\mathbf{x}, \mathbf{y}) n_j(\mathbf{x}) ds_x - \frac{1}{2} u_k(\mathbf{y}) \\
& + \int_{-a}^a \Delta u_i(x_1) \Sigma_{i2}^k(x_1, 0, \mathbf{y}; \omega) dx_1 + u_k^{\text{in}}(\mathbf{y}) = 0,
\end{aligned} \tag{4.4}$$

where $\mathbf{y} \in C_{BS}$ and $k = 1, 2$. Equation (4.4) is the regularized integral equation for the back surface, and it contains no worse than weakly singular integrals. In order to solve

the integral equation, the truncated back surface C_{BS} is used instead. The integrals over $C_{BS,\infty}$ are thus replaced by integrals over C_{BS} . For sufficiently large truncation limits T_1 and T_2 , this is expected to be a good approximation.

4.2. The integral equation for the crack. The integral equation for the crack is derived by applying Hooke's law (2.2) to an integral representation of the displacement, and then invoking the boundary condition on the crack. The integral representation of the displacement is derived in a manner analogous to the derivation of Eq. (4.1). With \mathbf{y} now an interior point so that no exclusion neighborhood is necessary, one obtains:

$$- \int_{C_{BS,\infty}} u_i(\mathbf{x}) \Sigma_{ij}^k(\mathbf{x}, \mathbf{y}; \omega) n_j(\mathbf{x}) ds_x + \int_{-a}^a \Delta u_i(x_1) \Sigma_{i2}^k(x_1, 0, \mathbf{y}; \omega) dx_1 + u_k^{\text{in}}(\mathbf{y}) = u_k(\mathbf{y}). \quad (4.5)$$

Since the singular point \mathbf{y} is not excluded, the right-hand side is now non-zero. Further, the integral over $C_{BS,\infty}$ is also here approximated by an integral over the truncated back surface C_{BS} . By applying Hooke's law (2.2) (with the gradient now taken with respect to \mathbf{y}), taking the limit $y_2 \rightarrow 0$ and invoking the boundary condition on the crack one obtains:

$$\begin{aligned} \lim_{y_2 \rightarrow 0} \sigma_{i2}(y_1, y_2) &= - \int_{C_{BS}} u_j(\mathbf{x}) \mathcal{C}_{i2kl} \frac{\partial}{\partial y_l} \Sigma_{jm}^k(\mathbf{x}, y_1, 0; \omega) n_m(\mathbf{x}) ds_x \\ &+ \lim_{y_2 \rightarrow 0} \int_{-a}^a \Delta u_j(x_1) \mathcal{C}_{i2kl} \frac{\partial}{\partial y_l} \Sigma_{j2}^k(x_1, 0, y_1, y_2; \omega) dx_1 \\ &+ \mathcal{C}_{i2kl} \frac{\partial}{\partial y_l} u_k^{\text{in}}(y_1, 0) = 0, \end{aligned} \quad (4.6)$$

where $i = 1, 2$, $|y_1| < a$ and \mathcal{C}_{ijkl} are the components of the elastic stiffness tensor \mathbf{C} in the coordinate system of the crack. It should be noted that the limit in front of the second integral cannot be moved inside the integral since the integrand is hypersingular [7, 9, 10]. This is expected, as noted above in the comment on the boundary condition on the crack. This problem is also automatically resolved by the solution method, as clarified in section 7.

5. PROBE MODELLING

The contact probes used in ultrasonic nondestructive testing usually consist of a piezoelectric crystal attached to a wedge. The wedge is typically made of a plastic material, and a couplant is usually applied between the wedge and the scanning surface of the component to increase the transmission of the emitted waves into the material. Following the 2D analogue of the model by Boström and Wirdelius [11], the action of a transmitting probe of this type can be modelled by prescribing the traction on the scanning surface underneath

it. For the transmitting probe (t), the boundary condition on the upper surface of the component is then taken as the traction:

$$\mathbf{t}^b = \begin{cases} A_0 i \mu k_p \left[\delta \sin 2\gamma \mathbf{e}_{x_1^b} + \left(\frac{k_s^2}{k_p^2} - 2 \sin^2 \gamma \right) \mathbf{e}_{x_2^b} \right] e^{-ik_p(x_1^b - t_1^b) \sin \gamma}, \text{ P probe,} \\ A_0 i \mu k_s \left[-\delta \cos 2\gamma \mathbf{e}_{x_1^b} + \sin 2\gamma \mathbf{e}_{x_2^b} \right] e^{-ik_s(x_1^b - t_1^b) \sin \gamma}, \text{ SV probe,} \end{cases} \quad (5.1)$$

beneath the surface of the probe (i.e. $|x_1^b - t_1^b| < w_1$ and $x_2^b = d + t_2^b$), and $\mathbf{t}^b = \mathbf{0}$ elsewhere. The two options are referred to as P probe and SV probe, respectively, since for $\delta = 1$ the tractions correspond exactly to the traction of a plane P or SV wave, respectively, restricted to the surface of the probe. The parameter δ accounts for the effect of the couplant applied between the wedge and the scanning surface: $\delta = 0$ represents fluid coupling and $\delta = 1$ a glued probe. Fluids of different viscosity can be modelled by setting an appropriate value of δ with $0 < \delta < 1$. The constant A_0 is the amplitude of the plane wave and γ is the angle of the probe, measured clockwise from the normal of the probe. This model of the transmitting probe can also be generalized to include the effect of a non-constant traction tapering off towards the edges of the probe. Since this effect is quite small that generalization is not made here, but it is discussed in the paper by Boström and Wirdelius [11].

The multiple scattering between the scanning surface and the crack and back surface is neglected, so the component can be regarded as half-infinite. To determine the incoming field it can then be expanded in P and SV plane wave potentials:

$$\mathbf{u}^{\text{in},b}(\mathbf{x}^b) = \nabla_b \varphi(\mathbf{x}^b) + \nabla_b \times \left(\psi(\mathbf{x}^b) \mathbf{e}_{x_3^b} \right), \quad (5.2)$$

where ∇_b denotes the nabla operator in the coordinate system of the back surface and the potentials $\varphi(\mathbf{x}^b)$ and $\psi(\mathbf{x}^b)$ are given by:

$$\begin{aligned} \varphi(\mathbf{x}^b) &= \frac{1}{2\pi} \int_{-\infty}^{\infty} A(q) e^{i(q(x_1^b - t_1^b) - h_p(x_2^b - t_2^b - d))} dq, \\ \psi(\mathbf{x}^b) &= \frac{1}{2\pi} \int_{-\infty}^{\infty} B(q) e^{i(q(x_1^b - t_1^b) - h_s(x_2^b - t_2^b - d))} dq. \end{aligned} \quad (5.3)$$

The Fourier transform of the traction vector given by Eq. (5.1) is:

$$\mathbf{T}^b = \begin{cases} A_0 i \mu k_p \left[\delta \sin 2\gamma \mathbf{e}_{x_1^b} + \left(\frac{k_s^2}{k_p^2} - 2 \sin^2 \gamma \right) \mathbf{e}_{x_2^b} \right] \frac{2 \sin(w_t(q + k_p \sin \gamma))}{q + k_p \sin \gamma}, \text{ P probe,} \\ A_0 i \mu k_s \left[-\delta \cos 2\gamma \mathbf{e}_{x_1^b} + \sin 2\gamma \mathbf{e}_{x_2^b} \right] \frac{2 \sin(w_t(q + k_s \sin \gamma))}{q + k_s \sin \gamma}, \text{ SV probe.} \end{cases} \quad (5.4)$$

Identification of the Fourier transform of the traction from the incoming field with Eq. (5.4) yields the functions $A(q)$ and $B(q)$:

$$\begin{aligned} A(q) &= \frac{2qh_s T_1^b + (2q^2 - k_s^2)T_2^b}{\mu R}, \\ B(q) &= \frac{(2q^2 - k_s^2)T_1^b - 2qh_p T_2^b}{\mu R}, \end{aligned} \quad (5.5)$$

where the Rayleigh function is $R = (2q^2 - k_s^2)^2 + 4q^2 h_p h_s$ and T_1^b and T_2^b are the components of the Fourier transformed traction vector \mathbf{T}^b given by Eq. (5.4). This determines the incoming field.

With the incoming field given by Eq. (5.2), solving the integral equations (4.4) and (4.6) yields the back surface and crack opening displacements. In order to model an ultrasonic testing situation it remains to relate these to the measured quantity - the output voltage of the receiving probe. For this purpose the electromechanical reciprocity relation by Auld [12] is ideal. It states that the change in transmission coefficient (or reflection coefficient in pulse-echo testing) due to a defect, as observed at the receiving probe (r) when the system is excited by an incident wave from the transmitting probe (t), is given by:

$$\delta\Gamma = \frac{-i\omega}{4P} \int_C (\mathbf{u}_2 \cdot \mathbf{t}_1 - \mathbf{u}_1 \cdot \mathbf{t}_2) ds. \quad (5.6)$$

Here \mathbf{u}_1 is the displacement and $\mathbf{t}_1 = (\mathbf{C} : \nabla \mathbf{u}_1) \cdot \mathbf{n}$ the corresponding traction when the transmitting probe (t) acts as a transmitter in the presence of the defect. The quantities \mathbf{u}_2 and $\mathbf{t}_2 = (\mathbf{C} : \nabla \mathbf{u}_2) \cdot \mathbf{n}$ are the corresponding displacement and stress when the receiving probe (r) acts as a transmitter in the absence of the defect. The probes are assumed to be transmitting at the angular frequency ω , and the quantity P is essentially the power supplied to the probe in transmitting mode. The contour C is any contour enclosing the defect, and \mathbf{n} is the inward unit normal vector of the contour. With $\delta\Gamma$ computed according to Eq. (5.6) the electric output signal $V_r(\omega)$ from the receiving probe (r) due to the scatterer is then given by:

$$V_r(\omega) = \delta\Gamma(\omega)V_t(\omega),$$

where $V_t(\omega)$ is the electric signal incident on the transmitting probe (t). The application of Auld's reciprocity relation to probe signal response calculations is discussed in more detail in the paper by Mattsson and Niklasson [13].

An application of Eq. (5.6) to the present case gives the change in transmission coefficient due to the crack as:

$$\delta\Gamma_C = \frac{-i\omega}{4P} \int_{-a}^a \Delta u_i(x_1) \sigma_{i2}^{\text{rc}}(x_1, 0) dx_1. \quad (5.7)$$

Here σ_{i2}^{rc} is the traction in the absence of the crack but in the presence of the back surface, when the receiving probe is transmitting. The COD Δu_i is due to an incoming field from the transmitting probe, in the presence of both the crack and back surface. The action of

the receiving probe acting as a transmitter is modelled in the same way as the transmitting probe.

An application of the reciprocity relation (5.6) also gives the change in transmission coefficient due to the back surface as:

$$\delta\Gamma_{BS} = \frac{i\omega}{4P} \int_{C_{BS}} u_i^{\text{re}}(\mathbf{x}) \sigma_{ij}^{\text{in}}(\mathbf{x}) n_j(\mathbf{x}) ds. \quad (5.8)$$

Here u_i^{re} is the displacement in the absence of the crack but in the presence of the back surface, when the receiving probe is transmitting. The stress σ_{ij}^{in} is the stress resulting from an incoming field from the transmitting probe (t), in the absence of both the crack and the back surface. It is computed by applying Hooke's law (2.2) to the incoming field given by Eq. (5.2).

It should be noted that all the computed $\delta\Gamma$ are computed for a fixed angular frequency, i.e. $\delta\Gamma = \delta\Gamma(\omega)$. In an experimental testing situation, the quantity of interest is the signal response as measured in the time domain. To obtain these time traces, an inverse Fourier transform of $\delta\Gamma_C(\omega)$ and $\delta\Gamma_{BS}(\omega)$ is taken with the frequency spectrum:

$$\frac{4\pi}{\omega_2 - \omega_1} \sin^2 \left(\pi \frac{\omega - \omega_1}{\omega_2 - \omega_1} \right) = \frac{1}{\Delta f} \cos^2 \left(\pi \frac{f - f_c}{2\Delta f} \right),$$

where f_c is the center frequency and Δf the 6 dB bandwidth.

6. DISCRETIZATION

In order to numerically solve the two coupled integral equations (4.4) and (4.6) for the crack opening and back surface displacements, three discretizations are introduced; (1): the COD $\Delta\mathbf{u}$ is expanded in a series of N Chebyshev functions, (2): the back surface C_{BS} is partitioned into N_e boundary elements with N_g geometrical nodes and approximated on each element by shape functions, (3): N_i interpolation nodes on the back surface are chosen and the displacement \mathbf{u} is approximated between the interpolation nodes on each element by interpolation functions. These discretizations yield a system of linear equations which are subsequently solved simultaneously for the $2N$ coefficients in the series expansion of the COD and the $2N_i$ displacements at the N_i interpolation nodes.

The series expansion of the COD in Chebyshev functions ψ_m is:

$$\Delta u_i(x_1) = \sum_{m=1}^N \alpha_{im} \psi_m(x_1/a), \quad (6.1)$$

where:

$$\psi_m(v) = \begin{cases} \frac{1}{\pi} \cos(m \arcsin v), & m = 1, 3, \dots, \\ \frac{1}{\pi} \sin(m \arcsin v), & m = 2, 4, \dots \end{cases}$$

These functions form a complete orthogonal set on $[-1, 1]$ with respect to the ordinary weighted L^2 -norm, with the weight function $(1 - v^2)^{-1/2}$. They also incorporate the correct square-root behaviour at the crack edges and satisfy a convenient integral property:

$$\int_{-1}^1 \psi_m(v) e^{-i\gamma v} dv = \frac{m}{\gamma} J_m(\gamma), \quad (6.2)$$

where J_m is the Bessel function of the first kind and order m . The use of the series expansion (6.1) in the truncated integral equation for the back surface (4.4) yields the equation:

$$\begin{aligned} & - \int_{C_{BS}} u_i(\mathbf{x}) [\Sigma_{ij}^k(\mathbf{x}, \mathbf{y}; \omega) - \Sigma_{ij}^k(\mathbf{x}, \mathbf{y})] n_j(\mathbf{x}) ds_x \\ & - \int_{C_{BS}} [u_i(\mathbf{x}) - u_i(\mathbf{y})] \Sigma_{ij}^k(\mathbf{x}, \mathbf{y}) n_j(\mathbf{x}) ds_x - \frac{1}{2} u_k^{\text{in}}(\mathbf{y}) \\ & + \sum_{m=1}^N \alpha_{im} \int_{-a}^a \psi_m(x_1/a) \Sigma_{i2}^k(x_1, 0, \mathbf{y}; \omega) dx_1 + u_k^{\text{in}}(\mathbf{y}) = 0, \quad k = 1, 2. \end{aligned} \quad (6.3)$$

Further, after inserting the series expansion (6.1) in the integral equation (4.6) and projecting on the expansion functions one obtains:

$$\begin{aligned} & - \int_{-a}^a \overline{\psi_n(y_1/a)} \left[\int_{C_{BS}} u_j(\mathbf{x}) \mathcal{C}_{i2kl} \frac{\partial}{\partial y_l} \Sigma_{jm}^k(x_1, x_2, y_1, 0; \omega) n_m(\mathbf{x}) ds_x \right] dy_1 \\ & + \sum_{m=1}^N \alpha_{jm} \lim_{y_2 \rightarrow 0} \int_{-a}^a \overline{\psi_n(y_1/a)} \left[\int_{-a}^a \psi_m(x_1/a) \mathcal{C}_{i2kl} \right. \\ & \times \left. \frac{\partial}{\partial y_l} \Sigma_{j2}^k(x_1, 0, y_1, y_2; \omega) dx_1 \right] dy_1 + \int_{-a}^a \overline{\psi_n(y_1/a)} \mathcal{C}_{i2kl} \frac{\partial}{\partial y_l} u_k^{\text{in}}(y_1, 0) dy_1 \\ & = 0, \quad i = 1, 2 \text{ and } n = 1, 2, \dots, N. \end{aligned} \quad (6.4)$$

where an overline is used to denote the complex conjugate. In order to get a square matrix the choice to project on N expansion functions is made in Eq. (6.4).

The boundary element discretization remains. In this paper an isoparametric interpolation (i.e. the shape and interpolation functions are the same and the geometrical nodes are used also as interpolation nodes) with quadratic Lagrangian interpolation functions is used. The BEM discretization is performed in the usual way, see e.g. Bonnet [6] and Domínguez [14]. For isoparametric interpolations $N_i = N_g$. Letting N_{node} denote this number, the use of quadratic interpolation functions implies that $N_{node} = 2N_e + 1$. By collocating Eq. (6.3) at the $2N_e + 1$ node points, $2(2N_e + 1)$ equations are obtained. Together with the $2N$ equations (6.4), one obtains a system of $2(2N_e + 1 + N)$ linear equations in $2(2N_e + 1 + N)$ unknowns: the $2(2N_e + 1)$ back surface displacements and the $2N$ series coefficients α_{im} .

After computing the incoming field and assembling and solving the discretized equations, it remains to compute the signal responses $\delta\Gamma_C$ and $\delta\Gamma_{BS}$ given by Eqs. (5.7) and (5.8). The computation of $\delta\Gamma_{BS}$ requires knowledge of the displacement u_i^{re} , i.e. the the back surface

displacement in the absence of the crack but in the presence of the back surface, with the receiving probe acting as transmitter. This displacement is computed by solving Eq. (6.3) with $N = 0$ (since the crack is absent) and the incoming field generated by the receiving probe (r). To compute $\delta\Gamma_{BS}$ once u_i^{re} is known, it remains to compute the stress σ_{ij}^{in} on the back surface by applying Hooke's law (2.2) to the incoming field given by Eq. (5.2), integrate the product $u_i^{\text{re}}\sigma_{ij}^{\text{in}}n_j$ on each boundary element and sum over the elements.

To compute $\delta\Gamma_C$, the series expansion (6.1) is used in Eq. (5.7) to give:

$$\delta\Gamma_C = \frac{-i\omega}{4P} \sum_{m=1}^N \alpha_{im} \int_{-a}^a \psi_m(x_1/a) \sigma_{i2}^{\text{re}}(x_1, 0) dx_1. \quad (6.5)$$

The coefficients α_{im} are known after solving the integral equations, and the traction σ_{i2}^{re} on the crack is computed by applying Hooke's law (2.2) to the truncated version of the integral representation (4.5) (with $\Delta u_i = 0$ since the crack is absent). The displacement u_i^{re} , which is known from the computation of $\delta\Gamma_{BS}$, is then used in the integral representation (4.5).

7. NUMERICAL EXAMPLES

In this section the numerical computations are discussed, and a few numerical examples are given to illustrate the model and the influence of the back surface.

The numerical computations are quite straightforward, owing mainly to the fact that the integral equation for the back surface is regularized and that the COD is computed with an analytically oriented method. Compared to an ordinary application of the BEM, the additional considerations required in the present hybrid method concern the choice of representation of the Green's tensors and the number of terms in the series expansion of the COD. Compared to an ordinary analytically oriented hypersingular integral equation method, the additional considerations required here mainly concern the truncation of the back surface and the length of the boundary elements.

In the computation of all integrals with dynamic Green's tensors in the integrand, in the integral equations (6.3) and (6.4), the choice between the closed Hankel form and the Fourier integral representation of the Green's tensor must be made. For the 2D SH case [4] these choices are discussed in detail, and the conclusions drawn there apply also to this case. Thus: in Eq. (6.3) the closed Hankel form is used throughout, whereas in Eq. (6.4) the closed Hankel form is used in the integral over the back surface while in the crack integral the Fourier representation is used instead. The Fourier representation has the benefit of enabling the application of the integral relation (6.2), thus reducing the order of integration by one for each application of the integral relation.

More important, however, is the fact that the use of the Fourier representation of the Green's tensor in conjunction with the integral relation (6.2) allows for an analytical treatment of the hypersingularity:

$$\begin{aligned} & \lim_{y_2 \rightarrow 0} \int_{-a}^a \overline{\psi_n(y_1/a)} \left[\int_{-a}^a \psi_m(x_1/a) \mathcal{C}_{i2kl} \frac{\partial}{\partial y_l} \Sigma_{j2}^k(x_1, 0, y_1, y_2; \omega) dx_1 \right] dy_1 \\ &= \frac{i\mu mn}{4\pi k_s^2} \int_{-\infty}^{\infty} \left[f_i(q) f_j(q) \frac{1}{h_p} + g_i(q) g_j(q) \frac{1}{h_s} \right] \frac{1}{q^2} J_m(aq) J_n(aq) dq, \\ & \qquad \qquad \qquad i, j = 1, 2 \text{ and } m, n = 1, 2, \dots, N. \end{aligned} \quad (7.1)$$

Here the functions $f_i(q)$ and $g_i(q)$ are defined by:

$$\begin{aligned} f_i(q) &= -\delta_{i1} 2qh_p + \delta_{i2} (k_s^2 - 2q^2), \\ g_i(q) &= \delta_{i1} (k_s^2 - 2q^2) + \delta_{i2} 2qh_s. \end{aligned} \quad (7.2)$$

In Eq. (7.1) the limit has been moved inside the integral, since it is convergent. This follows from the fact that for $i = j$ (the integrand is zero for $i \neq j$) the asymptotic behaviour of the integrand as $|q| \rightarrow \infty$ is:

$$\frac{f_i(q) f_i(q)}{h_p q^2} + \frac{g_i(q) g_i(q)}{h_s q^2} = \frac{2i(k_s^2 - k_p^2)}{|q|} + \mathcal{O}(|q|^{-3}). \quad (7.3)$$

To compute the integrals in Eq. (7.1) the range of integration is transformed to integration from 0 to ∞ , and the leading order terms are evaluated analytically using the relation:

$$\int_{-\infty}^{\infty} \frac{J_m(aq) J_n(aq)}{|q|} dq = \frac{\delta_{mn}}{m}.$$

The rest converges quickly enough for a direct numerical integration.

All integrals are computed numerically using Gauss-Legendre quadrature except the inverse temporal Fourier transform, which is computed using the trapezoidal rule. In all boundary element integrals, around 10 integration points are sufficient. An important consequence of the use of an isoparametric interpolation is that it enforces the Hölder continuity of \mathbf{u} which was assumed in the regularization of the integral equation (4.4). As a result, the singularity in the weakly singular integrals is cancelled and the integrals can be accurately computed using ordinary Gauss-Legendre quadrature.

For the outer integration in the first integral in (6.4), around 30 integration points are sufficient. In all other integrals, at the most 400 integration points are required. The integral relation (6.2) is used also for the last integral in Eq. (6.4). Regarding the truncation of the series expansion (6.1), the required number of terms grows with frequency so roughly $N = ak_s + 8$ terms seem to be enough.

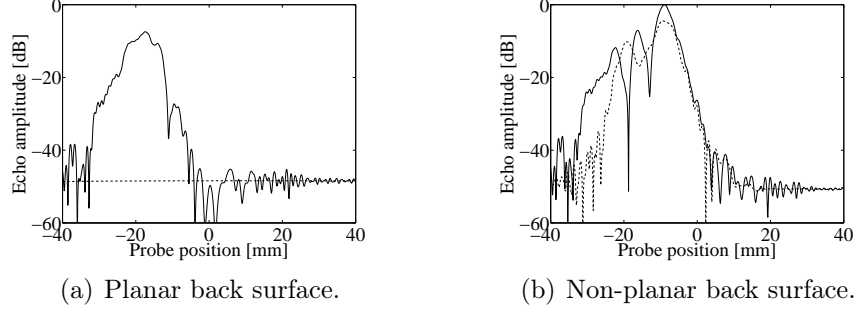


FIGURE 3. The echo amplitude as a function of probe position, crack angle $\beta = 90^\circ$. Solid curves (—): crack present, dashed curves (- -): crack absent.

In all the examples presented a pulse-echo testing situation (i.e. the same probe acting as both transmitter and receiver) is simulated and the back surface $g(x_1^b)$ is chosen as:

$$g(x_1^b) = \begin{cases} 0, & x_1^b < b, \\ \frac{A}{2} [1 + \sin(\frac{\pi}{c-b} (x_1^b - \frac{c+b}{2}))], & b \leq x_1^b \leq c, \\ A, & x_1^b > c, \end{cases}$$

where A , b , and c are defined in Fig. 1. In the numerical examples given, the parameters of the non-planar back surface are $A = 7.5$ mm, $b = -1$ mm and $c = 6.5$ mm. The Lamé constants of the material are $\lambda = 113.2$ GPa and $\mu = 80.9$ GPa, respectively, and the density is $\rho = 7900$ kg/m³. A 5 mm wide crack with $\beta = 90^\circ$ (i.e. vertical) or $\beta = 135^\circ$ is considered, and in both cases the crack center is located 5 mm from the lower part of the back surface. The probe is a 10 mm wide SV-probe with angle $\gamma = -45^\circ$ and fluid coupling so that $\delta = 0$. The probe is located at a vertical distance of 20 mm from the lower part of the back surface. Damping is incorporated in the model by giving the Lamé constants imaginary parts of 1% of the real parts.

The numerical results presented in this section were obtained for a back surface length of roughly 50 pressure wavelengths and boundary elements with a length of 1/4 of the Rayleigh wavelength. In the computation of the time traces 100 frequencies were used. These choices have been seen to generate good accuracy in the considered cases.

Figures 3 and 4 show the pulse-echo signal response as a function of probe position for crack angles $\beta = 90^\circ$ and $\beta = 135^\circ$, respectively. These signal responses were computed for a single frequency of 2 MHz. The results are not calibrated, but the same normalization is used so the results can be compared. In these figures the dashed curves show the signal response from the back surface in the absence of the crack, and the full-drawn curves show the total signal response with the crack present.

Figures 3(a) and 3(b) show the results for the vertical crack with a planar and non-planar back surface, respectively. As seen in Fig. 3(a) the crack gives a strong corner echo with an amplitude maximum for a probe position around 18 mm to the left of the crack. In the

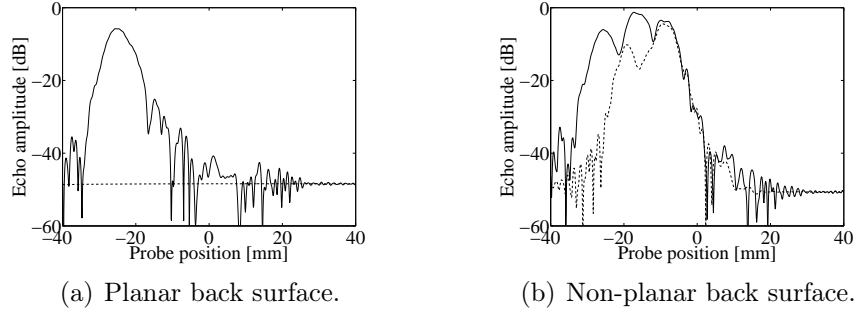


FIGURE 4. The echo amplitude as a function of probe position, crack angle $\beta = 135^\circ$. Solid curves (—): crack present, dashed curves (- -): crack absent.

case of the non-planar back surface in Fig. 3(b) the total amplitude maximum is instead attained for a probe position around 9 mm to the left of the crack, where the reflection by the back surface is strongest.

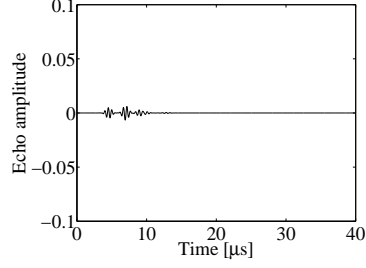
Figures 4(a) and 4(b) show the corresponding results for the crack with $\beta = 135^\circ$. A strong echo from the crack is observed in Fig. 4(a), with amplitude maximum for a probe position around 25 mm to the left of the crack. The results for the non-planar back surface in Fig. 4(b) show a strong echo with maximum for a probe position around 17 mm to the left of the crack. This maximum is stronger than for the planar back surface in Fig. 4(a), as expected due to a focusing effect of the non-planar part of the back surface which reflects incoming waves onto the crack and back to the probe.

It can also be noted in Figs. 3(a) and 4(a) that the planar back surface gives a very weak signal response which is also independent of probe position, as expected. The back surface signal response is also seen to be the same in Figs. 3(a) and 3(b) as in Figs. 4(a) and 4(b), respectively, as they must be since the back surface is the same.

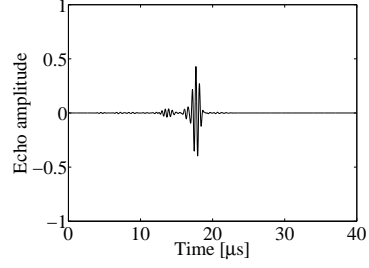
Figures 5 and 6 show the time traces for the cracks with $\beta = 90^\circ$ and $\beta = 135^\circ$, respectively, for a probe position 20.1 mm to the left of the crack center. The center frequency is $f_c = 2$ MHz and the 6 dB bandwidth is $\Delta f = 1$ MHz. The normalization is the same in all time traces, but it should be noted that the scale is different in the time traces for the planar back surface without the crack.

The time traces provide valuable means of checking the results, since the different contributions to the total signal response can be identified in these plots. This is discussed below for the results in Fig. 5, and an analogous analysis can be carried out to identify the pulses in Fig. 6. This is omitted here, but as noted above the back surface signal response must be identical regardless of crack angle. Accordingly, one may note that the time traces are the same in Figs. 5(a) and 5(c) as in Figs. 6(a) and 6(c), respectively.

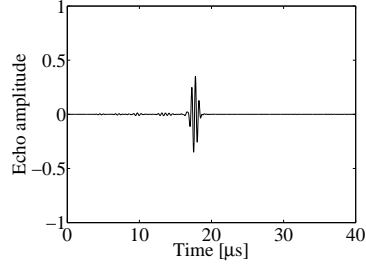
Figure 5(a) shows the time traces for the planar back surface without the crack. In the traces only the small fraction of the pulses reflected vertically by the back surface are



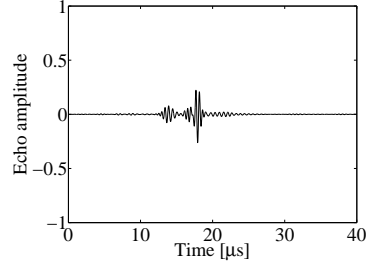
(a) Planar back surface, crack absent.



(b) Planar back surface, crack present.



(c) Non-planar back surface, crack absent.

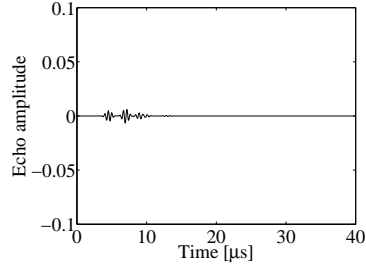


(d) Non-planar back surface, crack present.

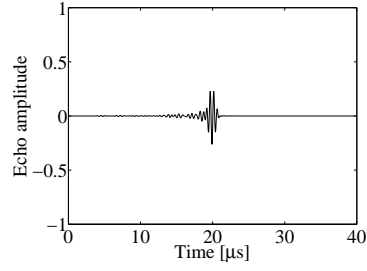
FIGURE 5. The time traces for a probe located 20.1 mm to the left of the crack, crack angle $\beta = 90^\circ$.

present, as expected. This wave path length corresponds to an arrival time of $t \approx 6.8 \mu\text{s}$ for a pure P-wave pulse, and this pulse is clearly visible in the traces. The mode converted pulses with arrival times of $t \approx 9.6 \mu\text{s}$ are also visible. The pure SV-wave pulse with an arrival time of $t \approx 12.5 \mu\text{s}$ is very weak since the coupling parameter $\delta = 0$, but a careful look reveals also this pulse in the traces.

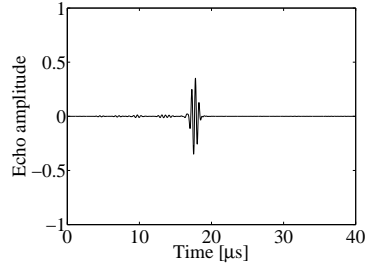
Figure 5(b) shows the time traces for the planar back surface with the vertical crack present. The pulses from the back surface are of course present also here, but the pure SV-wave pulse from the corner echo with a wave path length corresponding to an arrival time of $t \approx 17.9 \mu\text{s}$ now dominates the signal response. The corresponding pure P-wave pulse is much weaker since the probe is of SV type. This pulse, with an arrival time of $t \approx 9.7 \mu\text{s}$, also coincides with the mode converted pulses from the back surface mentioned above in connection to Figs. 5(a) and 5(b). In addition, the pure P-wave pulse which is diffracted by the lower crack tip and then reflected by the back surface also has an arrival time of $t \approx 9.6 \mu\text{s}$, and these three pulses are thus indistinguishable from each other. More apparent in the traces is the total contribution of the corner echo pulses from incoming SV-waves which are mode converted at the back surface (arrival time $t \approx 13.4 \mu\text{s}$) and on the crack (arrival time $t \approx 14.3 \mu\text{s}$), respectively. Finally, in contrast to the case in Fig. 5(a) with no crack, there are now also possibilities of multiple reflections between the crack



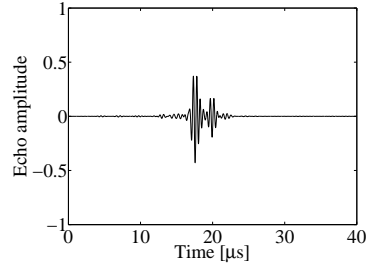
(a) Planar back surface, crack absent.



(b) Planar back surface, crack present.



(c) Non-planar back surface, crack absent.



(d) Non-planar back surface, crack present.

FIGURE 6. The time traces for a probe located 20.1 mm to the left of the crack, crack angle $\beta = 135^\circ$.

and back surface. These multiple reflections give rise to small pulses arriving late in the traces, as observed in Fig. 5(b).

The situation is more complicated for the non-planar back surface in Figs. 5(c) and 5(d). The time traces obtained in the absence of the crack, as shown in Fig. 5(c), feature the same pure P-wave pulse from the back surface arriving at $t \approx 6.8 \mu\text{s}$ as in the cases above, and the corresponding mode converted pulses and the pure SV-wave pulse are also present. However, the strong direct reflection by the non-planar part of the back surface of the pure SV-wave dominates the signal response, with a wave path length corresponding to an arrival time of $t \approx 17.7 \mu\text{s}$. The corresponding pure P-wave pulse arriving at $t \approx 9.6 \mu\text{s}$ is also present although impossible to distinguish in time from the mode converted pulses from the planar part of the back surface. Finally the mode converted pulses from direct reflection by the non-planar part of the back surface with arrival times of $t \approx 13.7 \mu\text{s}$ are also clearly visible in the figure.

Figure 5(d) shows the time traces for the non-planar back surface, with the crack present. As expected the weak reflections by the planar part of the back surface, discussed above, are present also here. In addition the corner echoes and the pulses reflected by the non-planar part of the back surface, all discussed above, are also present. However, since the

arrival times of these pulses coincide the different contributions cannot be distinguished. The mode converted corner echoes and pulses reflected by the non-planar part of the back surface are seen to generate a stronger signal response as compared to Figs. 5(b) and 5(c). In contrast, the pure SV-wave corner echo and reflection by the non-planar part of the back surface are seen to generate a weaker signal response in the same comparison. These effects are likely due to constructive and destructive interference, respectively, of the different pulses. Finally it can be noted that with a non-planar back surface more complex multiple reflections between the crack and back surface are possible than for the planar back surface, resulting in more and stronger pulses arriving late in the time traces.

8. CONCLUDING REMARKS

In this paper a 2D P-SV model of ultrasonic testing for interior strip-like cracks near a non-planar back surface is developed. The incident field emitted from an ultrasonic contact probe is modelled by prescribing the traction on the component beneath the probe. This enables the derivation of an explicit expression for the incident field in terms of an inverse Fourier transform. The wave scattering problem is solved by reformulating it as two coupled boundary integral equations for the unknown crack opening and back surface displacements. By using a combination of a series expansion of the crack opening displacement and a boundary element discretization of the back surface to solve the coupled integral equations, the hypersingularity in the BIE for the crack can be treated analytically while the geometry of the back surface is allowed to be quite arbitrary. The model is completed by employing an electromechanical reciprocity relation to model the action of the receiving probe and applying an inverse temporal Fourier transform to obtain the time traces.

The model presented in this paper treats the 2D in-plane case with a strip-like crack. In future research the 3D case with other types of defects will be treated.

ACKNOWLEDGMENTS

The work presented in this paper is sponsored by the Swedish Radiation Safety Authority (SSM) and this is gratefully acknowledged.

REFERENCES

- [1] R.K. Chapman. A system model for the ultrasonic inspection of smooth planar cracks. *J. Nondestr. Eval.*, 9:197–210, 1990.
- [2] P. Calmon, A. Lhémy, I. Lecœur-Taïbi, R. Raillon, and L. Paradis. Models for the computation of ultrasonic fields and their interaction with defects in realistic NDT configurations. *Nucl. Eng. Des.*, 180:271–283, 1998.
- [3] P. Bøvik and A. Boström. A model of ultrasonic nondestructive testing for internal and subsurface cracks. *J. Acoust. Soc. Am.*, 102:2723–2733, 1997.

- [4] J. Westlund. 2D SH modelling of ultrasonic testing for cracks near a non-planar surface. *Eng. Anal. Boundary Elem.*, 33:1103–1112, 2009.
- [5] S. Ström. Introduction to integral representations and integral equations for time-harmonic acoustic, electromagnetic and elastodynamic wave fields. In V.V. Varadan, A. Lakhtakia, and V.K. Varadan, editors, *Field Representations and Introduction to Scattering*, volume 1 of *Acoustic, electromagnetic and elastic wave scattering*. North-Holland, Amsterdam, 1991.
- [6] M. Bonnet. *Boundary Integral Equation Methods for Solids and Fluids*. John Wiley & Sons Ltd, Chichester, 1995.
- [7] V. Sladek and J. Sladek. Introductory notes on singular integrals. In *Singular Integrals in Boundary Element Methods* [15].
- [8] M. Guiggiani. Formulation and numerical treatment of boundary integral equations with hypersingular kernels. In Sladek and Sladek [15].
- [9] P.A. Martin and F.J. Rizzo. On boundary integral equations for crack problems. *Proc. R. Soc. London A*, 421:341–355, 1989.
- [10] P.A. Martin and F.J. Rizzo. Hypersingular integrals: How smooth must the density be? *Int. J. Numer. Methods Eng.*, 39:687–704, 1996.
- [11] A. Boström and H. Wirdelius. Ultrasonic probe modeling and nondestructive crack detection. *J. Acoust. Soc. Am.*, 97:2836–2848, 1995.
- [12] B.A. Auld. General electromechanical reciprocity relations applied to the calculation of elastic wave scattering coefficients. *Wave Motion*, 1:3–10, 1979.
- [13] J. Mattsson and A. J. Niklasson. Ultrasonic 2-D SH crack detection in anisotropic solids. *J. Nondestr. Eval.*, 16:31–41, 1997.
- [14] J. Domínguez. *Boundary Elements in Dynamics*. Computational Mechanics Publications, Southampton, 1993.
- [15] V. Sladek and J. Sladek, editors. *Singular Integrals in Boundary Element Methods*. Advances in Boundary Element Series. Computational Mechanics Publications, Southampton, 1998.

DEPARTMENT OF APPLIED MECHANICS, CHALMERS UNIVERSITY OF TECHNOLOGY, SE-412 96 GÖTEBORG, SWEDEN

E-mail address: jonathan.westlund@chalmers.se